Accepted for publication in Radio Science. To appear in 2001.

Use of GPS for estimation of bending angles of radio waves at low elevations

Sergey V. Sokolovskiy[1], Christian Rocken, and Anthony R. Lowry[2]

GPS Science and Technology Program, University Corporation for Atmospheric Research, Boulder, Colorado

Abstract. The paper compares three methods of calculating the bending angles of radio waves propagated from space to a ground-based receiver: (1) from refractivity climatology corrected for refractivity at the receiving antenna, (2) from radiosonde refractivity profiles, and (3) from the refractivity at the antenna and the measured Doppler frequency shift of the GPS signals. The methods are tested with the use of radiosonde and GPS observations collocated in space and in time. We analyzed seven cases during October-November 1999 where GPS satellites were observed to below 0.5° elevation from Point Loma, California, and which coincided closely in time with radiosonde launches from the nearby Miramar station. In all cases the bending angles calculated from Doppler and from radiosondes agree fairly well at all elevations, but in a number of cases both differ significantly at low elevations from the bending angles calculated from climatology corrected for the refractivity at the antenna. Thus GPS has the potential of being used for the correction of radar observations at low elevations instead of (or complementary to) radiosondes. The differences between the bending angles calculated from climatology corrected for the refractivity at the antenna and those calculated from the Doppler frequency shift indicate anomalies in the refractivity profile in the lower troposphere and can thus be used as an indicator of ducting conditions.

1. Introduction

The Global Positioning System (GPS), originally designed for precise timing and ranging, has found a wide range of applications in geodesy [*Herring,* 1996*; Dixon,* 1991] and meteorology [*Bevis et al.,* 1992; *Businger et al.,* 1996; *Ware et al.,* 1997]. In the radio occultation applications the excess phase delay between a GPS transmitter and receiver in space, induced by the Earth's atmosphere and ionosphere, is measured and used to solve the inverse problem of reconstructing profiles of atmospheric refractivity [*Melbourne, et al.,* 1994; *Kursinski et al.,* 1997; *Rocken et al.,* 1997]. In geodetic applications the observations must be corrected for the excess atmospheric phase delay which has to be modeled [*Herring,* 1996]. The excess phase delay as a function of time, i.e., Doppler frequency shift, is related to the arrival angle of radio waves. This has been routinely used in radio occultation data processing, where the bending angle as a function of impact parameter is calculated from the Doppler frequency shift of the radio signal and is then used for the reconstruction of refractivity as a function of altitude [*Fjeldbo et al.,* 1971]. The inverse problem of the reconstruction of refractivity profiles from radio signals received at the Earth's surface at positive elevation angles had been considered for a long time [*Kolosov and Pavel'yev,* 1982]. However, this problem is known to be ill conditioned and requires limiting the space of solutions in order to obtain feasible results [*Gaikovich and Sumin,* 1986; *Gaikovich,* 1992]. The reconstruction of bending angles from the Doppler frequency shift is an intermediate step in the reconstruction of refractivity, which is fairly well conditioned

(except at zero ray elevation at a receiver).

Bending angles can be estimated by a number of methods without GPS. Bending angles may be directly calculated with the use of (1) refractivity profiles derived from climatology, corrected for the refractivity measured at the receiving antenna, (2) refractivity profiles obtained from radiosondes, and (3) three-dimensional (3-D) refractivity fields obtained from numerical weather prediction (NWP) models. Method 1 can provide accurate results at elevations $\gtrsim 5°$, where the section of the ray inside the neutral atmosphere (where most of bending is accumulated) is much shorter than the Earth's radius. Under those conditions, sphericity of the atmosphere does not play a significant role, and the bending angle depends mainly on the refractivity at the receiving antenna, as in the case of a plain atmosphere [*Born and Wolf,* 1964]. At low elevations, where sphericity is not negligible, the bending angle depends on the whole refractivity profile, and the use of a radiosonde profile (method 2) provides better results than method 1. We note that the results of method 1 at low elevations depend on interpolation of refractivity between the surface value and climatology at higher altitudes. The optimal interpolation, which takes into account vertical correlation of refractivity in the lower troposphere for a given observational site, can provide best results in a statistical sense [*Gandin,* 1965]. However, all of the interpolation techniques may cause large errors under some unusual meteorological conditions. Both methods 1 and 2 assume the spherical symmetry of refractivity, while method 3 does not. It is difficult to determine whether method 3 is preferable to method 2 without accurate numerical simulations. Although method 3 has the advantage of accounting for horizontal gradients in refractivity, method 2, being an in situ observation, may better reproduce the vertical structure in refractivity which primarily affects the bending of radio waves at low elevations.

Calculation of bending angles from the Doppler frequency shift of the received GPS signals has the advantage of being a remote sensing technique which does not require the launching of radiosondes. Moreover, it can provide data almost continuously in time and at different azimuths, because the 24 GPS satellites rise 48 times and set 48 times per day at any location worldwide.

In this paper we consider the calculation of bending angles from the refractivity profile and from Doppler frequency shift of a received radio signal when the position and velocity of the transmitter are precisely known (GPS). Using radiosonde observations and GPS measurements that are collocated in space and in time and comparing the results, we find that in all cases the bending angles calculated from the radiosonde refractivity profile and from the GPS Doppler frequency shift are in good agreement. On the other hand, in a number of cases the bending angles calculated using the refractivity derived from climatology, corrected for the refractivity at the receiving antenna, differ significantly from both bending angles calculated from radiosondes and from Doppler at elevations $\lesssim 5°$. This indicates that GPS may be used for estimation of the bending angles of radio waves at low elevations instead of (or complementary to) radiosondes. The estimated bending angles can be used directly for the correction of the elevation angles of objects detected by radars when tracking those objects in space or at high enough altitudes. The difference between the bending angles at low elevations calculated from the Doppler frequency shift and from refractivity climatology corrected for the refractivity at the antenna can indicate anomalies in the refractivity profile in the lower troposphere; in particular, these differences may indicate the presence of atmospheric ducting conditions.

2. Calculation of Bending Angles From Refractivity Profile

Under the assumption of spherical symmetry of the refractivity the bending angle may be calculated by using Snell's law. The geometry of a ray, with all notations that will be used in this paper, is shown in Figure 1. Points 1 and 2 correspond to the receiver and transmitter, respectively. The center of sphericity is assumed to be at the center of local curvature of the Earth's reference ellipsoid at point 1. In the spherically symmetric case a ray is a plane curve, and its bending angle between any two points, e.g., points 1 and 2, is equal to

$$\alpha = \int_1^2 \frac{dl}{R_c} , \qquad (1)$$

where $dl = \sqrt{dr^2 + r^2 d\theta^2}$ is the differential of length and R_c is the local curvature radius of the ray. With the use of the expression for R_c in polar coordinates, $R_c = (r^2 + r'^2)^{3/2}/(r^2 + 2r'^2 - rr'')$, where $r' = dr/d\theta$, and with the use of the Snell's law [*Born and Wolf,* 1964],

$$\frac{r^2 n}{\sqrt{r^2 + r'^2}} = rn \sin\phi = a , \qquad (2)$$

where n is a refractive index and a is an impact parameter of the ray, the bending angle may be represented

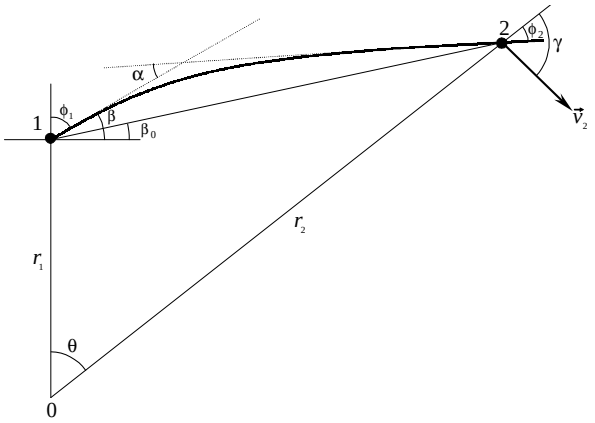

Figure 1. Geometry of a ray. Point 1 is a receiver. Point 2 is a transmitter or an arbitrary point on the ray. Point 0 is the center of curvature of the Earth reference ellipsoid under the receiver.

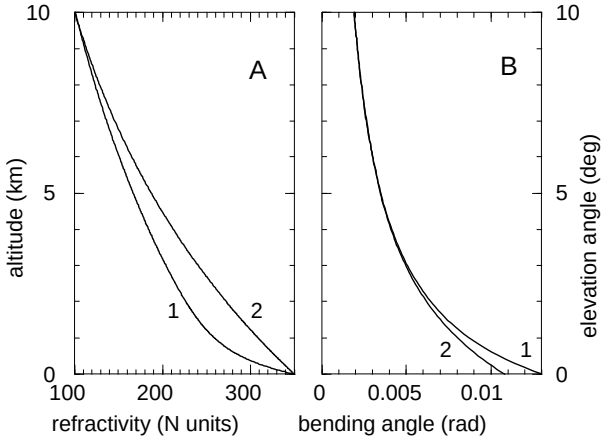

Figure 2. (a) Refractivity profiles having the same value at the surface. (b) Corresponding bending angle profiles.

in the form

$$\alpha = -a\int_{r_1}^{r_2} \frac{dn/dr}{n\sqrt{r^2n^2-a^2}}dr = -a\int_{x_1}^{x_2} \frac{dm/dx}{\sqrt{x^2-a^2}}dx \ , \tag{3}$$

where $x = rn(r)$ is a refractional radius and $m(x) = \ln\,[n(x)]$. Refractivity $N = 10^6(n-1)$ is a function of pressure P(mbar), temperature T(°K), and partial pressure of water vapor P_w(mbar) [*Bean and Dutton,* 1968]

$$N = 77.6\frac{P}{T} + 3.73\times 10^{-5}\frac{P_w}{T^2} \ . \tag{4}$$

We use P, T, and P_w as discrete functions of altitude z either from radiosondes or from climatological models. In this paper we use the version of the COSPAR International Reference Atmosphere which includes humidity, CIRA+Q [*Kirchengast et al.,* 1999]. We assume $r = r_e + z$, where r_e is the local curvature radius of the reference ellipsoid at the receiver site. We interpolate the discrete function $N_i = N(r_i)$ onto a denser grid with increment Δr, using either log-linear or log-spline interpolation, depending on the resolution of the data used (insufficient resolution of radiosonde data may cause artifacts when applying spline). The increment $\Delta r = 20$ m allows for calculation of $\alpha(a)$ using (3) with an accuracy of $\sim 10^{-8}$ rad for a CIRA+Q refractivity profile.

According to definition (1) the bending angle α does not depend on r_2 when r_2 is outside the atmosphere, i.e., $n(r_2) = 1$. In practice, however (e.g., when correcting the elevation angle of an object detected by a radar), it may be necessary to estimate the difference between the elevation angle of a ray arriving at the receiver, $\beta = \pi/2 - \phi_1$, and the elevation angle β_0 of the straight line between the receiver and an arbitrary point 2 on the ray where $n(r_2) = 1$, given the bending angle α. The difference $\Delta\beta = \beta - \beta_0$ depends on r_2 (it is strictly equal to α only when $r_2 = \infty$). Given α, ϕ_1, r_1, and r_2, the central angle θ between points 1 and 2 is equal to

$$\theta = \phi_1 - \phi_2 + \alpha = \phi_1 - \arcsin\,[r_1 n(r_1)\sin\phi_1/r_2] + \alpha \ . \tag{5}$$

Then the straight line elevation angle β_0 is

$$\beta_0 = \arctan\left(\frac{r_2\cos\theta - r_1}{r_2\sin\theta}\right) \ , \tag{6}$$

and this allows us to calculate $\Delta\beta$. When r_2 is not known but the distance l between r_1 and r_2 is known, then r_2 and θ, which are necessary to calculate β_0 by (6), may be obtained by concurrent solution of (5) and of the equation

$$l^2 = r_1^2 + r_2^2 - 2r_1r_2\cos\theta \ . \tag{7}$$

Equations (5) and (7) may be solved by use of an iterative method (which is computationally inexpensive).

Figure 2 shows examples of two refractivity profiles $N(z)$ which have the same value of $N(r_1)$ (Figure 2a) and the calculated profiles $\alpha(\beta_0)$ for $r_2 = 26,600$ km (Figure 2b). As seen, the difference in bending angles is significant at low elevations, and it decreases to zero

at higher elevations, where the bending angle depends mainly on $N(r_1)$.

3. Calculation of Bending Angles From Doppler Frequency Shift

The relation of the bending angle of radio waves to the Doppler frequency shift (derived in different ways) is given, e.g., by *Kolosov and Pavel'yev* [1982], *Gaikovich* [1992], and *Vorob'ev and Krasil'nikova* [1994]. The bending angle is calculated in the reference frame where the refractive medium (the atmosphere) is at rest. The Doppler frequency shift of the signal is related to the projections of the velocity vectors of the transmitter and receiver onto the directions of the wave propagation (normal to wave fronts). In the case of a ground-based receiver its velocity is equal to zero. Then the Doppler frequency shift of the received signal, f_d, under the assumption of spherical symmetry of refractivity is equal to

$$f_d = -f v_2 c^{-1} \cos(\gamma - \phi_2) , \qquad (8)$$

where f is the carrier frequency, c is light velocity in vacuum, and γ is the angle between the vertical direction at the receiver and the projection of the receiver velocity vector $\mathbf{v}_2$ on the ray plane (as shown in Figure 1). Equation (8) allows us to calculate ϕ_2 from the measured f_d,

$$\phi_2 = \gamma - \arccos(-f_d c / f v_2) . \qquad (9)$$

The angle ϕ_1, which is also necessary for calculating the bending angle, can be obtained from Snell's law (2),

$$\phi_1 = \arcsin[r_2 \sin\phi_2 / r_1 n(r_1)] . \qquad (10)$$

Then the bending angle α is equal to

$$\alpha = \theta - \phi_1 + \phi_2 . \qquad (11)$$

In the case of GPS, $\mathbf{r}_1$, $\mathbf{r}_2$, $\mathbf{v}_2$, and, thus, θ and γ, are precisely known, which allows for the calculation of α by means of (9)-(11) with sufficient accuracy. We note that when calculating ϕ_1 by means of (10), it is impossible to distinguish between positive and negative ray elevation angles β at the receiver. This introduces an ambiguity in the bending angle α. To resolve this ambiguity, it is necessary to begin the processing of GPS data at high enough elevations, where β is known to be greater than 0, and to calculate the impact parameter $a = r_2 \sin\phi_2$. Zero elevation angle, $\beta = 0$, corresponds to a maximum in a. After the maximum in a has been passed, the angle ϕ_1, as formally calculated from (10), must be replaced by $\pi - \phi_1$.

4. Error Analysis

In this paper, which is primarily a feasibility study, we present a preliminary analysis of the main error sources. A more detailed error analysis, which accounts for the main potential error source, horizontal inhomogeneity of refractivity in the troposphere, is a complicated problem that must be addressed in a separate paper.

An observational error in the Doppler frequency shift δf_d results in the corresponding error in bending angle $\delta\alpha$, which can be approximately obtained by varying (9)-(11) and by keeping the linear terms,

$$\delta\alpha = -\frac{r_2 c \cos\phi_2}{r_1 v_2 \cos\phi_1 \sin(\gamma - \phi_2)} \frac{\delta f_d}{f} . \qquad (12)$$

Similarly, the observational error in refractivity at the receiving antenna $\delta N(r_1)$ causes the bending angle error

$$\delta\alpha = 10^{-6} \tan\phi_1 \delta N(r_1) . \qquad (13)$$

As seen from (12) and (13), formally (in linear approximation), $\delta\alpha \to \infty$ when $\phi_1 \to \pi/2$, and it indicates that the problem of calculation of the bending angles from Doppler is ill conditioned at zero ray elevation at the receiver, $\beta = 0$. In practice, however, the higher-order terms of expansion of (10), which were not taken into account in (12) and (13), result in a finite error $\delta\alpha$.

For a GPS signal received at the Earth's surface, f_d is on the order of $\sim 10^3$ Hz, which is mainly related to the motion of the GPS satellite. The excess Doppler frequency shift Δf_d, i.e., the portion of f_d which is caused by refraction (i.e., slowing and bending) of radio waves, is on the order of ~ 1 Hz. Assuming that the station coordinates and the GPS orbits are well known and that millimeter-level GPS phase measurement noise can be neglected, the main sources of the observational error in Doppler, δf_d, are GPS and receiver clock errors and multipath. GPS transmitter frequency is known to $\sim 10^{-12}$ or better. Errors of the receiver clock can also be reduced to $\sim 10^{-12}$ or better by use of a stable oscillator at the receiver, by differencing receiver clock errors, by estimating the receiver clock error, or a combination of these. For the GPS carrier frequency, $\sim 10^9$ Hz, this translates into an error $\delta f_d \sim 10^{-3}$ Hz. The error δf_d due to the multipath can vary greatly depending on the antenna environment. The magnitude of the phase error due to the multipath depends on the amplitude of the reflected signal A_r and can be approximately estimated as $(\lambda/2\pi) \arcsin(A_r/A_0)$, where λ is the wavelength and A_0 is the amplitude of the direct GPS signal. The period of the multipath error depends on the position of the reflector with respect

to the antenna and the direction of the GPS transmitter. For observations over a sea (like those used in this study) the main source of the multipath is reflection from the water surface. The difference in phase path between direct and reflected signals at low elevations is approximately equal to $2h\beta$, where h is the height of antenna above the sea surface. Thus the period of the multipath error is equal to $\lambda[2h(d\beta/dt)]^{-1}$. Assuming $h = 10$ m and an inclination of the GPS satellite orbit of 50° ($d\beta/dt = (1^\circ/2\,\mathrm{min})\cos 50^\circ$), the period of the multipath error is about ~100 s. Assuming further a large reflection coefficient for seawater of $A_r/A_0 \sim 0.9$, the magnitude of the phase error is ~3.5 cm. Thus the magnitude of the Doppler error δf_d is $\sim 10^{-2}$ Hz. Reflections from a glassy seawater surface introduce the worst case multipath error. Multipath reflections from a rough sea surface are much reduced. The magnitude of the oscillating multipath error can also be reduced by filtering (see section 5). We note further that several techniques are under development to reduce the effects of multipath. For example, in the case of a small number of multiple tones with large enough amplitudes (like reflections from the sea surface) their effect on the phase may be reduced with a correction that is based on the spectral analysis of the measured amplitude [*Axelrad et al.,* 1996].

Refractivity at the GPS antenna can be measured with a standard meteorological sensor with an accuracy of ~2 N units (see section 5). It is possible that this error can be reduced by using several sensors around the antenna and by averaging their observations.

Figure 3 shows the bending angle error $\delta\alpha$ as a function of β_0, for (1) $\delta f_d = 10^{-3}$ Hz (clock error), (2) $\delta f_d = 10^{-2}$ Hz (peak magnitude of the worst case oscillating multipath error), and (3) $\delta N(r_1) = 2$ N-units (routine observational error of refractivity at the antenna).

Additional errors in bending angles are induced by horizontal gradients in the refractivity field that violate the assumption of spherical symmetry (horizontal homogeneity) which is used in the calculation of the bending angles. Errors caused by refractivity irregularities with large enough scales can be evaluated by ray tracing through realistic 3-D models of refractivity in the lower troposphere (as was done for the estimation of the phase delay [*Chen and Herring,* 1997]). In the moist lower troposphere (in the midlatitudes and, especially, in the tropics), horizontal inhomogeneity in refractivity is mainly induced by the complicated spatial structure of water vapor. It is likely that the largest errors may be induced by small-scale irregularities of

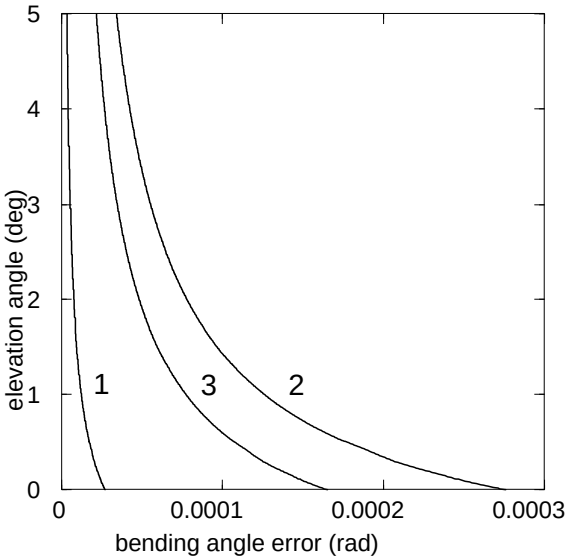

Figure 3. Bending angle error corresponding to (1) Doppler error 10^{-3} Hz (GPS and receiver clock errors), (2) 10^{-2} Hz (peak magnitude of the worst case multipath oscillating error), and (3) refreactivity error at antenna 2 N units (routine measurement error).

humidity in the area around the antenna. The impacts of these small-scale irregularities may differ, depending on their shape. For example, a small bulge of humidity centered at the antenna may have only an insignificant effect on the direction of wave propagation. However, ϕ_1 calculated from (10) will be affected through the measured refractivity at the receiving antenna $N(\mathbf{r}_1)$. Thus the effect of such a humidity bulge is equivalent to the observational error $\delta N(r_1)$. Evaluation of the effect of small-scale refractivity irregularities is a complicated problem in part because the small-scale humidity structures are not well reproduced by atmospheric models. The most robust system-level error evaluation of the technique described in this paper can be obtained by direct comparison of the GPS-estimated bending angles to those measured independently by radars tracking targets with accurately known position.

5. Processing of GPS and Radiosonde Observational Data

For this feasibility study we computed GPS bending angles from several test cases in October-November 1999. For only a small number of cases did the GPS receiver track usable data to below 0.5°. For an even smaller number of cases did we have correlative ra-

diosonde data within a few hours from the nearby Miramar radiosonde site. For the seven cases that we processed and compared, the bending angles calculated from GPS and from radiosondes agree fairly well at all elevations, but in a number of cases both differ significantly at low elevations from bending computed from climatology and corrected for refractivity at the receiving antenna. This paper illustrates this with three selected example cases: Two cases show results under conditions of atmospheric ducting, and one case shows the results for "normal" atmospheric conditions.

GPS data were collected from a pier overlooking the Pacific Ocean on the Point Loma peninsula near San Diego, California, latitude 32.697°N, longitude 117.254°W. Observables were collected with an AOA SNR-8000 receiver retrofitted with Benchmark ACT^{TM} tracking. The receiver clock was steered by a Datum FTS1195 crystal oscillator, with nominal 5×10^{-13} short-term stability. The antenna, a Dorne-Margolin choke ring fitted with a special high-gain preamplifier, was tilted $\sim$30° in the direction of the ocean. The antenna altitude over the ocean surface was 13 m.

GPS observables were processed using the Bernese version 4.2 software [*Rothacher and Mervart*, 1996] in a precise point positioning mode [e.g., *Zumberge et al.*, 1997]. Single-path observations are required for atmospheric sensing applications, and we examined methods for inverting single-path measurements from differenced observables [e.g., *Alber et al.,* 2000] but found point positioning to be more feasible for observations at low elevation angles $\lesssim$5°, primarily because no suitable high-rate and low-elevation observations from other GPS tracking sites could be found for differencing. Precise point positioning requires precise ephemerides and high-rate satellite clock estimates. We used Jet Propulsion Laboratory (JPL) orbits and 1/30 Hz clock solutions [*Zumberge et al.*, 1998]. Ground-based GPS observations are typically sampled at 1/30 Hz, but this rate is insufficient for numerical differentiation of the phase (which must be filtered to remove high-frequency noise in the measurements). Consequently, we sampled the data at a rate of 1 Hz. To process at 1 Hz, we initially attempted to interpolate the 1/30 Hz satellite clocks. However, clock errors due to selective availability (SA) were aliased sufficiently by 1/30 Hz sampling to introduce significant ($\gtrsim$2 cm s^{-1} rate) errors in excess phase. Thus we first solved for 1 Hz satellite clock rates using point positioning at three 1 Hz sites in the International GPS Service (IGS) global network (FAIR in Alaska, KOKB in Hawaii, and GODE in Maryland), and we then used those clock corrections to interpolate the JPL 1/30 Hz clock solutions. Since this study was conducted, SA has been turned off, and our data processing for the estimation of bending angles from ground-based GPS observations has become significantly simpler.

The parameter estimation for data collected at the Point Loma site included (1) epochwise solution of the receiver clock error, (2) phase ambiguity estimation from combined carrier phase and smoothed code observables, and (3) solution for zenith wet delay at half-hourly intervals. The site coordinates were held fixed to a geodetic network solution, and dry atmospheric delay was modeled from the surface pressure measurements using the Niell mapping function [*Niell,* 1996]. Ionospheric dispersive delay was removed by linear combination of excess phases, s_1 and s_2 at the two GPS carrier frequencies, $f_1 = 1.57542$ GHz and $f_2 = 1.2276$ GHz [*Melbourne et al.*, 1994],

$$s = (f_1^2 s_1 - f_2^2 s_2)/(f_1^2 - f_2^2) \; . \qquad (14)$$

The Bernese software was modified for this application to provide on output the position vector of the receiver $\mathbf{r}_1$, the position and velocity vectors of the GPS satellite $\mathbf{r}_2(t)$ and $\mathbf{v}_2(t)$ (all in a common Earth-fixed reference frame), the measured excess phase path s (consisting of the sum of excess phase from the dry delay model, the wet delay parameterization, and the parameter estimation residuals), and the refractivity at the receiver (from the meteorological measurements). Excess phase can be determined only to within a small uncertain constant (of the order of centimeters) because, in the precise point positioning method, phase ambiguities are estimated but cannot be resolved to integer values. As a result, our excess phase estimates may be biased. However, this is of no consequence because only the derivative is needed to estimate Doppler frequency, $\Delta f_d = -fc^{-1}ds/dt$.

Owing to the coastal setting of our experiment, the GPS phase observables are subject to strong multipath effects from reflections off the ocean surface. Significant reductions in signal strength at times of maximum multipath interference commonly result in loss of s_2 phase data for short periods [e.g., *Anderson*, 1994], particularly when a satellite is at low elevation. In addition to the missing data, i.e., gaps, the observational data also contain cycle (half cycle) slips which most likely occur under the conditions of low signal power. A combination of different numbers of simultaneous slips in s_1 and s_2 can produce a slip of different magnitude in s. We use a filtering technique which we specially designed for processing of the data with gaps and cycle slips.

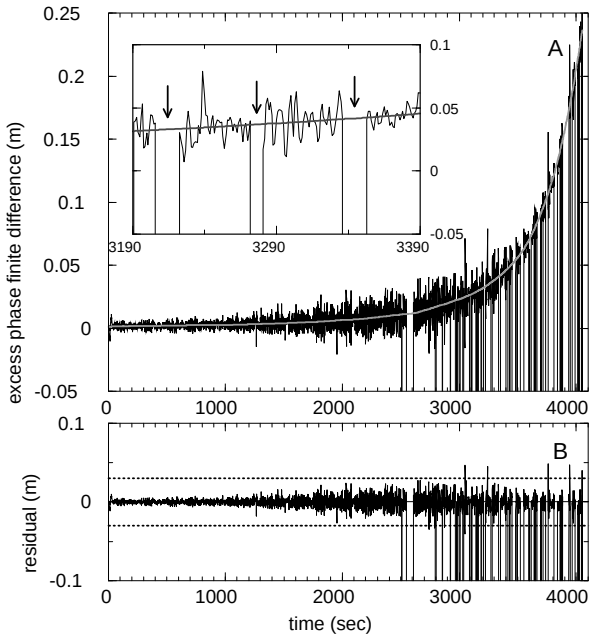

Figure 4. (a) Excess phase finite difference ("Doppler") before and after the filtering. (b) Residual of the "Doppler" after the first filtering.

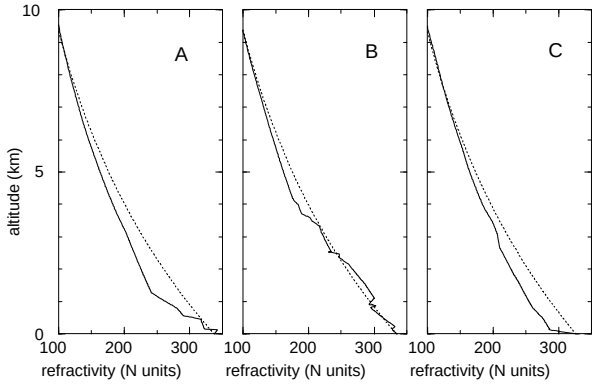

Figure 5. Solid lines, radiosonde refractivity profiles collocated with ground-based GPS observations; dashed lines, exponential interpolation of refractivity between the surface and CIRA+Q at 10 km. (a) November 11, 00 UTC, (b) November 20, 12 UTC, (c) December 6, 00 UTC, 1999.

Without cycle slips it would be possible to filter the raw phase and then to calculate Doppler by differentiation. With cycle slips it appears more expedient to first directly calculate Doppler through the finite difference of phases (then the cycle slips expose themselves as spikes) and then to subject it to filtering. We use combined filtering which consists of two steps, and we apply it two times. The first step is the cubic spline regression (which is a least squares fit to the raw data by natural cubic spline specified on a sparser grid than the raw data). This spline regression eliminates the main trend in data and interpolates through gaps. The second step is Fourier filtering of the difference between the raw data and the spline regression (this difference is set to zero inside gaps). Figure 4a shows the results of this combined filtering of raw excess phase finite difference, which we will call, for brevity, Doppler in this paragraph. In the case of missing excess phase data (gaps) the raw Doppler was set to -999, and thus the gaps are framed by descending vertical lines. The gray thick line shows the filtered Doppler. The graph inset shows a magnified section of the raw and filtered Doppler which allows to better view the interpolation through gaps (indicated by arrows). The residual Doppler, which is the difference between the raw and the filtered Doppler, is shown in Figure 4b. This residual clearly shows a number of spikes after ~3000 s. By assuming that those spikes are caused primarily by half-cycle slips we remove them from the data (replaced by -999) on the basis of a ±3 cm tolerance criterium (shown by dashed lines in Figure 4b). The Doppler with the eliminated spikes is then subjected to the second filtering and then used for the calculation of bending angles. The filter bandwidth was taken as 0.01 Hz, which approximately corresponds to a 1° smoothing window in the elevation angle domain.

Radiosonde data were used from the station Miramar, located at 32.87°N latitude, 117.15°W longitude ~20 km to the NNE of the receiver. Surface meteorological data were collected at 5 min intervals by a Paroscientific Met3 sensor situated ~12 m from the GPS antenna. The bottom altitude of the radiosonde profiles was 134 m. The refractivity measured at the surface was merged with the radiosonde profiles using exponential interpolation. Figures 5a, 5b, and 5c show with solid lines three refractivity profiles calculated from the radiosonde and surface data. Dashed lines show the refractivity profiles obtained by exponential interpolation between the refractivity measured at the GPS receiver antenna location and CIRA+Q refractivity at 10 km. Above 10 km, as well as above the top of the radiosonde profiles, only CIRA+Q refractivity was used. As seen, in Figure 5b the CIRA+Q profile corrected for the refractivity at the receiving antenna is rather close to the radiosonde profile, while in Figures 5a and 5c the

difference is noticeably larger in the lower troposphere.

Accuracy of the radiosonde and the surface refractivity measurements was ∼2 N units. In the lower troposphere at the site of our observations the error is apportioned about half and half between the first,"dry," and the second, "wet," terms in (4) (in the dry troposphere the error can be ∼1 N unit, and in the moist tropical troposphere it can be ∼3-4 N units). An additional error can be introduced by horizontal inhomogeneity of tropospheric refractivity. Refractivity can vary horizontally along the ray from the receiving antenna toward the GPS satellite. In the comparisons presented in this study an additional error is introduced due to the variation of refractivity along 20 km distance between the GPS antenna and the radiosonde launch site. As was already mentioned in section 4, the analysis of errors induced by horizontal inhomogeneity of the refractivity is a complicated problem and is beyond the scope of this feasibility study.

As seen from (3), the bending angle is mostly sensitive to the refractivity gradient. When calculating the bending angle from a radiosonde refractivity profile, the bending error depends on the magnitude and correlation radius of the refractivity error. If we assume that errors at all radiosonde observation altitudes are not correlated (worst case), then the bending angle error depends mainly on the refractivity error at antenna altitude. In particular, for our observations, when the next observational altitude is ∼130 m above the antenna height, a 2 N units refractivity error at the GPS antenna results in $\sim 1.5\times10^{-4}$ rad of bending angle error at zero elevation. For correlated errors of 2 N units at all altitudes the bending angle at zero elevation is much smaller, $\sim 2\times10^{-5}$ rad.

Figures 6a, 6b, and 6c show the bending angle profiles calculated from the GPS Doppler frequency shift (thick solid lines) and from the refractivity profiles shown in Figures 5a, 5b, and 5c (from the radiosonde refractivity, thin solid lines; from CIRA+Q corrected for the refractivity at antenna, dashed lines). As seen, the bending angles calculated from the GPS Doppler frequency shift agree fairly well in all cases with those calculated from the radiosonde data. Meanwhile, estimation of the bending angles from climatology corrected for refractivity at the receiving antenna provides good results above ∼5° and, in some cases (when the climatology-based refractivity profile does not differ significantly from the true one), at lower elevations (Figure 6b). In other cases, when the difference between the true and the climatology-based refractivity profiles is significant (ducting or close to ducting conditions),

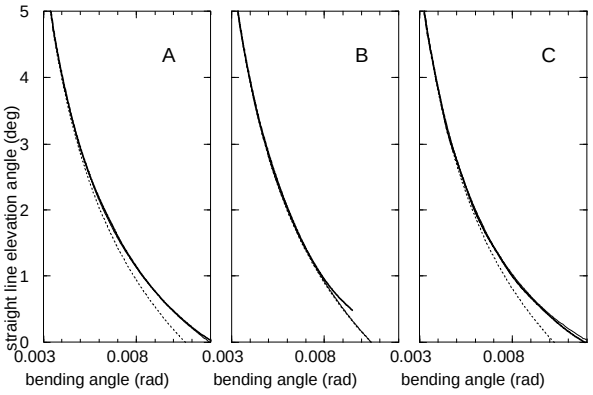

Figure 6. Bending angle profiles. Thick solid lines, calculated from Dopller frequency shift of the received GPS signals for (a) November 10, 20:52 UTC, (b) November 20, 14:19 UTC, and (c) December 5, 23:37 UTC; thin solid lines, calculated from the radiosonde refractivity profiles; dashed lines, calculated from the refractivity profiles interpolated between the surface and CIRA+Q at 10 km.

estimation of the bending angles from Doppler yields significantly better results at low elevations. The difference between the bending angles at low elevations calculated from Doppler and from climatology indicates anomalies in the refractivity profile in the lower troposphere. In particular, when the bending angles calculated from Doppler are larger than those calculated from climatology, this may indicate ducting or close to ducting conditions.

In the cases shown in Figures 6a and 6c the signal was tracked down to negative elevation angle of the GPS, while in the case shown in Figure 6b, tracking stopped at ∼0.5° elevation angle. Often, prior to declaring loss of lock, the GPS receiver tracks with large errors. That might explain the discrepancy between the GPS and the radiosonde bending angles between 0.5° and 1° in Figure 6b. Tracking of GPS down to low enough elevation can by itself indicate a high probability of ducting or close to ducting conditions. For more reliable tracking of GPS signals at low elevations an open-loop technique with the use of the predicted Doppler model should be applied [*Sokolovskiy,* 2001].

6. Conclusions

The results of this feasibility study show that precise measurements of the Doppler frequency shift of GPS

signals observed with a ground-based receiver allow estimation of the bending angles of radio waves at low elevation angles. The bending angles calculated from the Doppler frequency shift of the received GPS signals are in good agreement with the bending angles calculated from the radiosondes and often are in disagreement at low elevations with the bending angles calculated from climatology corrected for the refractivity at the receiving antenna. Thus the bending angles estimated from Doppler frequency shift of GPS signals may be used for angular correction of radar observations at low elevations without (or complementary to) radiosondes.

The results presented here are postprocessed, but real-time application of this technique appears feasible. Predicted GPS orbits and clocks are available from the International GPS Service (IGS) to compute excess phases in real time [*Springer and Hugentobler*, 2000]. Velocity errors and clock frequency errors of these predictions need to be further investigated to carefully evaluate the real-time errors of the technique. Other errors in bending angles calculated from Doppler frequency shift depend primarily on receiver clock errors, and on site-specific multipath conditions. For low-multipath environments the bending angle error can be on the order of $\sim 10^{-5}$ rad ($\sim 6 \times 10^{-4}$ deg). Worst case multipath (like the reflection from the sea surface considered in section 4) can introduce oscillating errors with a peak magnitude of $\sim 2.8 \times 10^{-4}$ rad ($\sim 1.6 \times 10^{-2}$ deg) at 0° elevation and $\sim 1.3 \times 10^{-4}$ rad ($\sim 7 \times 10^{-3}$ deg) at 1° elevation. However, the multipath error can be substantially reduced by (1) choosing low-multipath environment, (2) low-pass filtering of the observational Doppler, and (3) correction for the reflected signals with the use of the spectral analysis of amplitude. Refractivity measurement errors at the antenna of ~ 2 N units result in a bending angle error of $\sim 1.7 \times 10^{-4}$ rad ($\sim 10^{-2}$ deg) at 0° elevation and $\sim 7 \times 10^{-5}$ rad ($\sim 4 \times 10^{-3}$ deg) at 1° elevation. It is possible that this error can be reduced by using several refractivity sensors around the antenna and by averaging their observations. Estimation of the errors of bending angles introduced by the horizontal inhomogeneity of refractivity in the lower troposphere, including the effect of small-scale irregularities of moisture in the boundary layer, has yet to be done. The difference in bending angles calculated from Doppler frequency shift and from climatology corrected for the refractivity at the receiving antenna indicates anomalies of the refractivity profile in the lower troposphere; in particular, it can be used as an indicator of ducting conditions.

Acknowledgments. This work was sponsored by the Office of Naval Research, Scott Sandgathe, code 322MM. The authors are grateful to Kenneth Anderson for help with data collection and for useful discussion of the subject. We also thank Teresa VanHove for data processing support. Two anonymous referees greatly helped to improve the paper with constructive comments.

References

Alber, C., R. Ware, C. Rocken, and J. Braun, Inverting GPS double differences to obtain single path phase delays, *Geophys. Res. Lett., 27*, 2661-2664, 2000.

Anderson, K.D., Tropospheric refractivity profiles inferred from low-elevation angle measurements of Global Positioning System (GPS) signals, *AGARD Conf. Proc., AGARD-CP-567-2*, 1-6, 1994.

Axelrad, P., C.J. Comp, and P.F. MacDoran, SNR based multipath error correction for GPS differential phase, *IEEE Trans. on Aerosp. Electron. Syst., 32*(2), 650-660, 1996.

Bean, B.R., and E.J. Dutton, *Radio Meteorology*, 423 pp., Dover, Mineola, N. Y., 1968.

Bevis, M., S. Businger, T. A. Herring, C. Rocken, R. A. Anthes, and R. H. Ware, GPS meteorology: Remote sensing of atmospheric water vapor using the Global Positioning System, *J. Geophys. Res., 97*(D14), 15,787-15,801, 1992.

Born, M., and E. Wolf, *Principles of Optics: Electromagnetic Theory of Propagation, Interference, and Diffraction of Light*, Pergamon, New York, 856 pp., 1964.

Businger, S., S.R. Chiswell, M. Bevis, J. Duan, R. A. Anthes, C. Rocken, R. H. Ware, T. VanHove, and F. S. Solheim, The promise of GPS in atmospheric monitoring, *Bull. Am. Meteorol. Soc., 77*, 5-18, 1996.

Chen, G., and T. A. Herring, Effects of atmospheric azimuthal asymmetry on the analysis of space geodetic data, *J. Geophys. Res., 102*(B9), 20,489-20,502, 1997.

Dixon, T.H., An introduction to the Global Positioning System and some geological applications, *Rev. of Geophys., 29*(2), 249-276, 1991.

Fjeldbo, G., A.J. Kliore, and V.R. Eshleman, The neutral atmosphere of Venus as studied with the Mariner V radio occultation experiments, *Astron. J., 76*(2), 123-140, 1971.

Gaikovich, K.P., Ground-based Doppler radio-frequency refractometry of the atmosphere, *Radiophys. and Quantum Electron., 35*(3-4), 149-154, 1992.

Gaikovich, K.P., and M.I. Sumin, Reconstruction of the altitude profiles of the refractive index, pressure, and temperature of the atmosphere from observations of the astronomical refraction, *Izv. Russ. Acad. Sci. Atmos. Oceanic Phys., 22*, 710-715, 1986.

Gandin, L.S., *Objective Analysis of Meteorological Fields*, 242 pp., Isr. Program for Sci. Transl., Jerusalem, 1965.

Herring, T., The Global Positioning System, *Sci. Am.*, 44-50, 1996.

Kirchengast, G., J. Hafner, and W. Poetzi, The CIRA86aQ_UoG model: An extension of the CIRA-86 monthly tables including humidity tables and a Fortran95 global moist air climatology model, *IMG/UoG Techn. Rep. for ESA/ESTEC, 8*, Eur. Space Agency, Paris, France, 1999.

Kolosov, M.A., and A.G. Pavel'yev, Radio transillumination of the atmosphere by artificial and natural sources, *J. Commun. Technol. Electron., 27*(12), 30-37, 1982.

Kursinski, E.R., G.A. Hajj, J.T. Schofield, R.P. Linfield, and K.R. Hardy, Observing Earth's atmosphere with radio occultation measurements using the Global Positioning System, *J. Geophys. Res., 102*(D19), 23,429-23,465, 1997.

Melbourne, W.G., E.S. Davis, C.B. Duncan, G.A. Hajj, K.R. Hardy, E.R. Kursinski, T.K. Meehan, L.E. Young, and T.P. Yunck, The application of spaceborne GPS to atmospheric limb sounding and global change monitoring, *JPL Publ. 94-18,* 147 pp., 1994.

Niell, A.E., Global mapping functions for the atmospheric delay at radio wavelengths, *J. Geophys. Res.*, *101*(B2), 3227-3246, 1996.

Rocken, et al., Analysis and validation of GPS/MET data in the lower troposphere, *J. Geophys. Res.*, *102*(D25), 29,849-29,866, 1997.

Rothacher, M., and L. Mervart (Eds.), Bernese GPS software version 4.0, Astron. Inst., Univ. of Berne, Bern, Switzerland, 1996.

Sokolovskiy, S.V., Tracking tropospheric radio occultation signals from low Earth orbit, *Radio Science,* in press, 2001.

Springer, T.A., and U. Hugentobler, IGS Ultra rapid products for near-real-time applications, *Eos Trans., AGU, 81*(48), Fall Meet. Suppl., F320, 2000.

Vorob'ev, V.V., and T.G. Krasil'nikova, Estimation of accuracy of the atmospheric refractive index recovery from Doppler shift measurements at frequencies used in NAVSTAR system, *Izv. Russ. Acad. Sci. Atmos. Oceanic Phys., 29*, 602-609, 1994.

Ware, R., C. Alber, C. Rocken, and F. Solheim, Sensing integrated water vapor along GPS ray paths, *Geophys. Res. Lett., 24*, 417-420, 1997.

Zumberge, J.F., M.B. Heflin, D.C. Jefferson, M.M. Watkins, and F.H. Webb, Precise point positioning for the efficient and robust analysis of GPS data from large networks, *J. Geophys. Res., 102*(B3), 5005-5017, 1997.

Zumberge, J.F., M.M. Watkins, and F.H. Webb, Characteristics and applications of precise GPS clock solutions every 30 seconds, *Navigation, 44*(4), 449-456, 1998.

A. R. Lowry, C. Rocken, and S. V. Sokolovskiy, University Corporation for Atmospheric Research, P.O. Box 3000, Boulder, CO 80307-3000 (arlowry@ucar.edu; rocken@ucar.edu; sergey@ucar.edu)

[1]Also at A. M. Obukhov Institute of Atmospheric Physics, Moscow

[2]Now at Department of Physics, University of Colorado, Boulder

Received August 8, 2000; revised December 28, 2000; accepted January 10, 2001.